

COMPARATIVE STUDY OF TiO<sub>2</sub> AND ZnO APPLICATION IN HYBRID SOLAR CELLS USING COPOLYMER P3OT/P3MTLetícia Fernanda Gonçalves Larsson<sup>a</sup>, Gideã Taques Tractz<sup>a</sup>, Guilherme Arielo Rodrigues Maia<sup>a</sup>, Guilherme José Turcatel Alves<sup>b</sup>, Paulo Rogério Pinto Rodrigues<sup>a,\*</sup>, Maico Taras da Cunha<sup>a</sup> and Everson do Prado Banczek<sup>a</sup><sup>a</sup>Departamento de Química, Universidade Estadual do Centro Oeste, 85040-080 Guarapuava – PR, Brasil<sup>b</sup>Instituto Federal de Roraima, 69303-340 Boa Vista – RR, Brasil

Recebido em 21/09/2018; aceito em 11/12/2018; publicado na web em 23/01/2019

Hybrid inorganic-organic solar cells are an attractive alternative energy source because of their low-cost production and ability to make use of a large amount of solar radiation available. This work aims to evaluate different solar cells composed of TiO<sub>2</sub> and ZnO with P3OT/P3MT copolymer. Layers of semiconductor oxides were deposited on transparent fluorine-doped tin oxide (FTO) by spin coating and adsorption in the polymer solution. X-ray diffraction (XRD), scanning electron microscopy (SEM), were used to characterize the fabricated semiconductors and curves of current density vs. potential (j-V), photochromoamperometry (j-t) and electrochemical impedance spectroscopy (EIS) were used to determine their electrical characteristics. The XRD analyses confirmed the crystalline nature of the oxide materials. SEM micrographs showed the spherical morphology of ZnO and the poorly defined agglomerate morphology of TiO<sub>2</sub>. The electrochemical measurements proved that the best cell was produced with P3OT/P3MT copolymer and TiO<sub>2</sub>, owing to its lower charge transfer resistance, with the following photovoltaic parameters:  $V_{oc} = 0.615 \text{ V} \pm 0.004$ ,  $j_{sc} = 1.545 \text{ mA cm}^{-2} \pm 0.240$ ,  $FF = 0.637 \pm 0.003$ , and  $\eta = 0.617\% \pm 0.117$ .

Keywords: semiconductor; renewable energy; photochromoamperometry.

## INTRODUCTION

Hybrid solar cells are composed of three main materials: an organic material capable of absorbing of solar energy, a metallic semiconductor to allow for the transport of electrons, and a redox electrolyte for charge intermediation. The hybrid solar cells were initially developed in 1985 and are based on the formation of electron-hole pairs, connected to each other, generating an electric field derived from the separation of charges at the interface of the system.<sup>1</sup>

When the incident light reach the device, electrons from the photosensitive material are ejected by the photovoltaic effect to the lowest unoccupied molecular orbital (LUMO) state and consequently to the conduction band of semiconductor.<sup>2</sup> These electrons migrate to the external circuit because of the potential difference at the device interface until they reach the counter electrode (Pt); the polymer is regenerated via a diffusion process, thus completing the charge injection cycle and causing current to flow.<sup>3</sup>

Semiconductor oxides such as TiO<sub>2</sub>, ZnO, Nb<sub>2</sub>O<sub>5</sub>, and CeO<sub>2</sub> are used in these devices because they possess good photochemical properties, thermodynamic stability, great crystallinity a form transparent films invisible light and presents band gap in the order of 3 to 3.4 eV.<sup>4,5</sup> They are often used in combination with photosensitizing materials because it is necessary to take advantage of some effective interactions between both materials.<sup>5</sup>

Poly (3-alkylthiophenes) (P3ATs) are organic polymers with conjugated structures, which make them conductive and luminescent. They are considered promising alternative sensitizer materials for solar cells and in organic electronics, because they are highly flexible, are easy to produce, have low processing costs, have high mobility and are efficient charge generators ( $0.1 \text{ cm}^2 \text{ V}^{-1} \text{ s}^{-1}$ ).<sup>1</sup>

P3ATs can be obtained from the monomers of 3-octylthiophene (3OT) and 3-methylthiophene (3-MT) and are characterized by the

presence of a thiophene ring containing a methyl or an octyl radical attached to the carbon at position 3 of ring 9, as shown in Figure 1.<sup>6</sup>

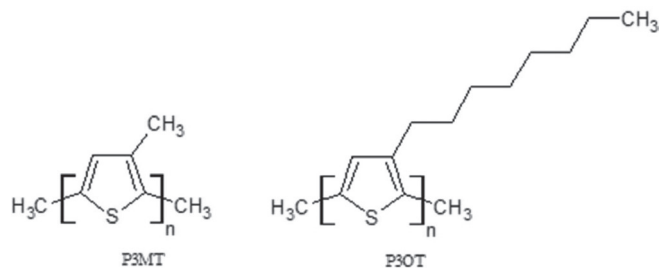


Figure 1. Chemical structure of poly(3-methylthiophene) (P3MT) and poly(3-octylthiophene) (P3OT) respectively

Because P3ATs have alternating single ( $\sigma$ ) and double ( $\pi$ ) bonds, the overlapping of  $p_z$  orbitals causes a delocalization of  $\pi$  bonds along the chain-forming degenerate bonding and anti-bonding orbitals. Consequently, quasi-continuous energy levels are formed, and the bands formed by degeneracy are called the valence band (VB) and conduction band (CB). The energetic difference between the valence and conduction bands (bandgap) determines if the polymer is conductive, semiconductive, or insulating.<sup>1,7</sup>

Use of thiophene copolymers (a combination of two or more polymers) has already been demonstrated and was studied by Freitas *et al.*,<sup>8</sup> who observed their advantages compared to those of obtained by using the individual polymers separately, but no comparative studies of the use of different oxides have been published as yet.

This work aims to produce and electrochemically characterize hybrid solar cells produced with ZnO and TiO<sub>2</sub> oxides using poly(3-octylthiophene) and poly(3-methylthiophene) (P3OT/P3MT) as a sensitized copolymer.

\*e-mail: prprodriues@gmail.com

## EXPERIMENTAL SECTION

### ZnO particle synthesis

ZnO particles were synthesized by a coprecipitation method (Figure 2).<sup>9</sup>

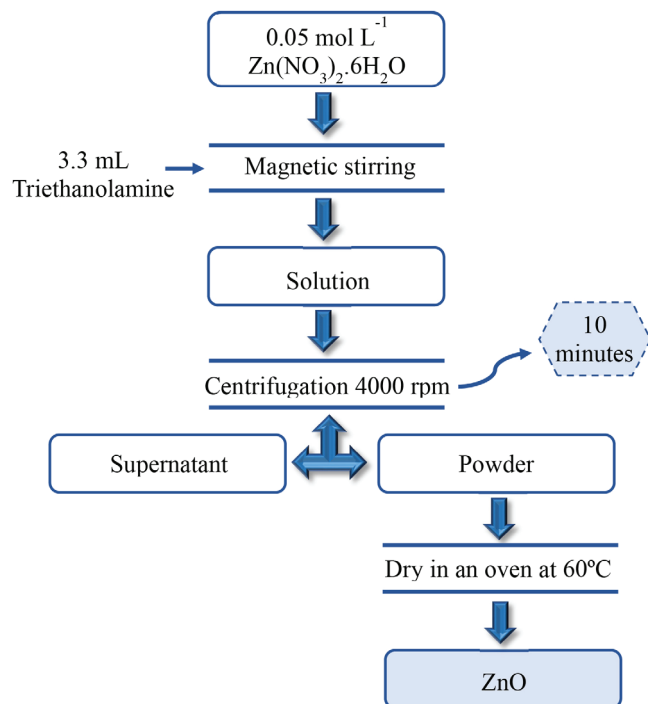


Figure 2. Flow chart for the ZnO synthesis by coprecipitation method

### Solar cell fabrication

#### Counter electrode

Platinum electrodeposited on FTO was used as the counter electrode. Three electrodes were used in the electrochemical cell: an Ag/AgCl reference electrode, a platinum plate counter electrode, and an FTO working electrode. The electrolytic solution was prepared with  $\text{K}_2\text{PtCl}_6$   $1 \times 10^{-4}$  mol L<sup>-1</sup> in 0.1 mol L<sup>-1</sup> of HCl. The cyclic voltammetric deposition was performed in four cycles with a potential range of E varying from -0.5 V to 0.5 V at a scanning speed of 20 mV s<sup>-1</sup>.

#### Photoanode

The working electrode was constituted from the synthesized ZnO or TiO<sub>2</sub> (Sigma-Aldrich, 25 nm particle size) deposited over fluorine-doped tin oxide (FTO) substrates. To deposit oxides on FTO, a suspension was produced consisting of: 3 g of ZnO or TiO<sub>2</sub>, 0.1 mL of Triton X-100 (VETEC), 0.1 mL of 99.5% acetylacetone (VETEC) and 4 mL of bidistilled H<sub>2</sub>O.<sup>10</sup> The deposition of the films was performed by spin coating at 2500 rpm for 20 s with 3 consecutive layers. After the depositions, the films were heated at 450 °C for 30 min.<sup>11</sup> The ZnO and TiO<sub>2</sub> coated films after calcination were immersed in a P3OT/P3MT solution for 24 h to adsorption.<sup>7</sup>

#### Solar cell

The solar cell was assembled in a “sandwich” form, with the photoanode and counter electrode joined and an electrolytic solution between the plates. The electrolyte used consisted of 0.1 mol L<sup>-1</sup> LiI, 0.05 mol L<sup>-1</sup> I<sub>2</sub>, and 0.5 mol L<sup>-1</sup> 4-tert-butyl pyridine in acetonitrile. The active cell area was measured to be 0.2 cm<sup>2</sup>, as shown in Figure 3.

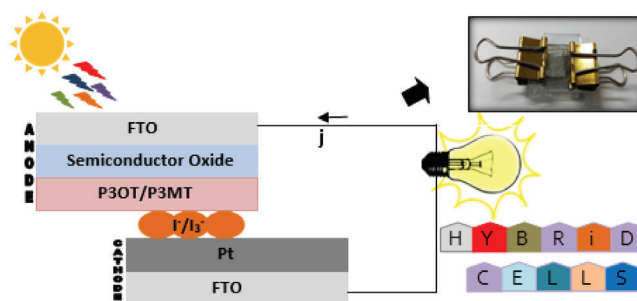


Figure 3. Schematic diagram of the solar cell structure

### Characterization of ZnO and TiO<sub>2</sub> structures

Powder X-ray diffraction (XRD) patterns were recorded as Bruker DRX D2 Phaser instrument using CuK<sub>α</sub> radiation source with a wavelength of 1.5 nm operated at 30 kV and 10 mA, a scan speed of 0.5° s<sup>-1</sup>, using a LynxEye detector. The diffraction angle was varied from 20° to 75°.

Scanning electronic microscopy (SEM) images were collected with a TESCAN® VEGA3 SEM with an SE detector and a tungsten filament at 20 kV and a working distance of 10 mm.

### Electrochemical characterization of solar cells

The characterization of the solar cell systems was performed in a Zahner potentiostat, Zennium Electrochemical Workstation model, linked to XPot and a LOT Oriel—Quantum Design GmbH-solar simulator, with a xenon lamp and a beam diameter of 25 mm. The measurements were performed under illumination of 100 mW cm<sup>-2</sup> within a cell area of 0.2 cm<sup>2</sup>, with a standard solar spectrum at AM 1.5G.

Electrochemical impedance spectroscopy (EIS) measurements were performed over a frequency range of 10 kHz–0.01 Hz. The perturbation potential applied was ±10 mV relative to V<sub>oc</sub>. Photochronoamperometry measurements were performed for 660 s, with the lamp being interrupted in intervals of 60 s.

Current versus potential curves (j-V) were measured to obtain the photovoltaic parameters of the cells and calculate the energy conversion efficiency of the systems.

## RESULT AND DISCUSSION

Figures 4 and 5 shows the X-ray diffractograms of TiO<sub>2</sub> and ZnO particles, respectively.

The TiO<sub>2</sub> used presented peaks characteristic of single phase crystalline anatase particles. The main and most intense peak was observed at a 2θ angle of 25.30° can be indexed to the (101) plane, while the other diffraction peaks observed at 37.82°, 48.04°, 53.91°, 55.08°, 62.62°, 68.70°, and 7.41°, are the (112), (200), (105), (211), (204), (116), and (220) planes of the TiO<sub>2</sub> anatase unit cell.<sup>11</sup> The observed peaks were narrow and well-defined, indicating the organized structure of a crystalline and homogeneous powder. No secondary peaks were observed, which affirmed the high purity of TiO<sub>2</sub>.<sup>12</sup> The cataloging of the peaks was performed by comparison with the crystallographic record PDF 71-1166 using EVA® software referring to TiO<sub>2</sub> anatase phase.

XRD was used to identify crystalline phases and the XRD results confirmed that the ZnO particles consisted of a wurtzite crystalline phase,<sup>13</sup> with intense diffraction peaks at 2θ values of 31.78°, 34.78°, and 36.30°, which correspond, respectively, to the (100), (002), and (101) planes, and peaks at 2θ values of 47.83°,

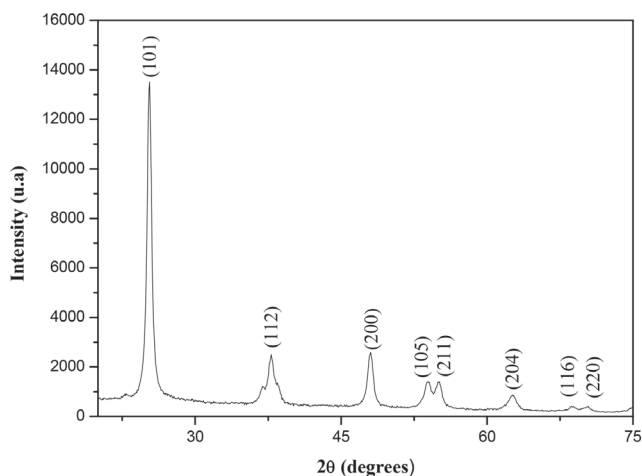


Figure 4. X-ray diffractogram of anatase TiO<sub>2</sub> particles

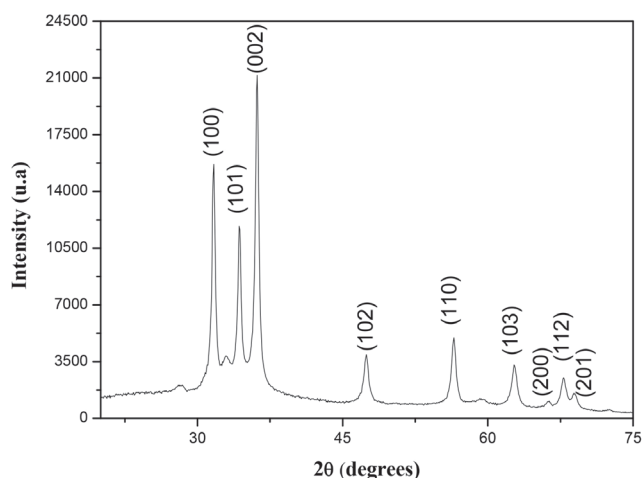


Figure 5. X-ray diffractogram of ZnO particles synthesized by co-precipitation

56.52°, 63.12°, 66.78°, 67.89°, and 69.37°, which can be indexed to the (102), (110), (103), (200), (112), and (201) planes, respectively, indicating the unitary cells in a hexagonal compact system that are characteristic of ZnO.<sup>14</sup>

The diffractogram (Figure 5) shows only primary peaks; there were no peaks that did not belong to ZnO, indicating that the crystals were of high crystallinity and free from impurities. The obtained peaks are narrow, well-defined, and intense, indicating a high degree of structural organization and consequently, a crystalline and homogeneous powder.<sup>15</sup> The cataloging of the peaks was performed by comparison with the crystallographic record PDF 01-075-0576 using EVA software, referring to pure ZnO.

Figure 6 shows SEM images of the oxide samples being analyzed.

In Figure 6, the SEM images demonstrate the spherical morphology of the synthesized ZnO and the particles presented mean sizes of  $600 \pm 100$  nm. The morphology of the ZnO particles is very sensitive to factors such as the reaction time, concentration and synthesis temperature.<sup>16</sup> This spherical morphology is characteristic of the coprecipitation method and precursor concentration used. Fan *et al.*,<sup>17</sup> reported nanosphere formation from this production method using others precursors, specifically hexamethylenetetramine, (CH<sub>2</sub>)<sub>6</sub>N<sub>4</sub>, zinc nitrate (Zn(NO<sub>3</sub>)<sub>2</sub>), and Na<sub>3</sub>C<sub>6</sub>H<sub>5</sub>O<sub>7</sub>, as a surfactant.<sup>18</sup>

The TiO<sub>2</sub> particles did not exhibit a well-defined morphology, instead of taking the form of clusters. According to Costa *et al.*,<sup>19</sup> Pratsinis,<sup>20</sup> and Hong *et al.*,<sup>21</sup> particles smaller than 1 μm tend to agglomerate because of the high surface energy associated with the extensive surface area of such small particles. Muniz *et al.*<sup>22</sup> proved that TiO<sub>2</sub> anatase presented a higher clustering density and higher surface area per unit volume in relation to the rutile phase and the brookite phase, increasing its use as an electron acceptor.<sup>23,4</sup>

In order to evaluate the cell response to the incident light, EIS measurements were performed for the devices in the presence of light, and the results are presented in the Nyquist diagram (Figure 7).

The Nyquist diagram shows that for the ZnO+P3OT/P3MT solar cell there is only one capacitive arc with higher impedance values than those observed for the TiO<sub>2</sub>+P3OT/P3MT cell. The impedance response indicates that the ZnO cell presents greater resistance to the photocurrent generation processes.

Three capacitive arcs were seen for the TiO<sub>2</sub>+P3OT/P3MT cell. The first arc, at high frequency, corresponds to the charge transfer process in the platinum counter electrode. In the intermediate frequency region, there is a second capacitive arc related to the charge recombination process and electrons transport in the conduction band of the working electrode.

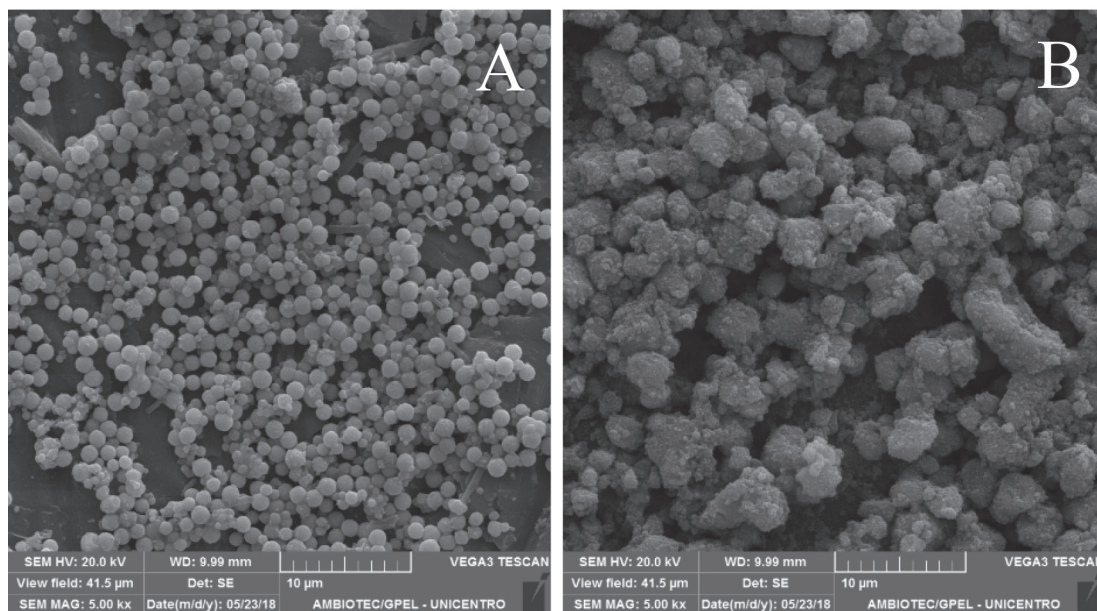
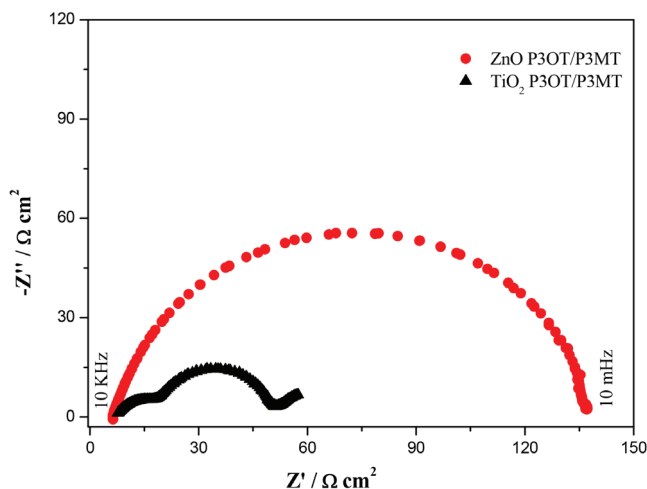


Figure 6. SEM images of (a) ZnO and (b) TiO<sub>2</sub>



**Figure 7.** Nyquist type EIS diagram obtained for solar cells of ZnO and TiO<sub>2</sub> with P3OT/P3MT copolymer under illumination of 100 mW cm<sup>-2</sup>

The third arc can be observed at low frequencies and is related to the Nernstian diffusion process in the electrolyte, I/I<sub>3</sub><sup>-</sup>. This process of electron transfer with I<sub>3</sub><sup>-</sup> ions occurs at the semiconductor/electrolyte interface.<sup>22</sup>

It is observed variations in the diameter of the semicircles corresponding to changes in the charge transfer resistance of the film with different oxides. The TiO<sub>2</sub>+P3OT/P3MT cell presented the smallest semicircle, indicating the lowest resistance to charge transfer, showing TiO<sub>2</sub>+P3OT/P3MT to be more photosensitive than ZnO+P3OT/P3MT.

The TiO<sub>2</sub>+P3OT/P3MT cell presented a capacitive arc corresponding to the platinum counter electrode, indicating better injection of electrons on the surface of the semiconductor and consequently a greater efficiency in photon collection. ZnO cells are known to only present a capacitive arc when inefficient cells are produced, usually using dyes derived from biomass, which are poor devices for energy conversion.<sup>24-26</sup>

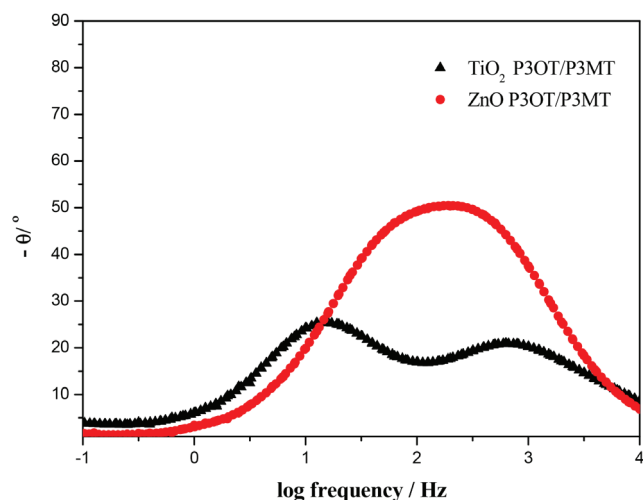


**Figure 8.** EIS diagram of the Bode phase angle obtained under 100 mW cm<sup>-2</sup> illumination of ZnO and TiO<sub>2</sub> solar cells with P3OT/P3MT copolymer

The Bode phase angle diagrams (Figure 8) present three-time constants for the TiO<sub>2</sub>+P3OT/P3MT solar cell. The first constant, observed at a frequency of 1000 Hz, is associated with the charge transfer process on the platinum counter electrode with a phase angle of 20°. The second time constant, observed in the 1-Hz frequency

region, corresponds to charge recombination and processes that involve the transport of electrons in the conduction band of the working electrode with a phase angle of 26°. The third constant might be observed at frequencies between 0.1 and 0.01 Hz and is assigned to the Nernstian diffusion process in the I/I<sub>3</sub><sup>-</sup> electrolyte, with a phase angle of 7°.

For the ZnO+P3OT/P3MT cell, three-time constants were observed, but the processes could not be clearly separated. A region of constant phase angle that can be observed between frequencies of 1000 and 100 Hz is associated with an overlap of the charge transfer processes in the platinum counter electrode and charge recombination and electron transport in the conduction band of the working electrode.

Charge transfer in the counter electrode was noted at 300 Hz for the ZnO+P3OT/P3MT cell with a phase angle of 49.2°. For this cell, charge recombination and electron transport in the conduction band of the working electrode were observed at 85 Hz with a phase angle of 48.6°. The time constant for the Nernstian diffusion in the I/I<sub>3</sub><sup>-</sup> electrolyte was between 0.1 Hz and 0.01 Hz with a phase angle of 3°.

In the TiO<sub>2</sub> cell, the displacement to higher frequencies with lower phase angles of the time constant for charge transfer in the counter electrode indicates a faster response in the photocurrent generation with a higher efficiency. This response, at lower frequencies and lower phase angles for recombination and electron transport, indicates that in the TiO<sub>2</sub> cell, the electron lifetime is longer and the recombination processes are less favored compared to the ZnO solar cell. The lower phase angle values determined for the diffusion process in the ZnO cell indicates the recombination of injected electrons, regenerating the copolymer and minimizing electrolyte diffusion.

In Figure 9, the photochronoamperometry measurements for the systems are analyzed.

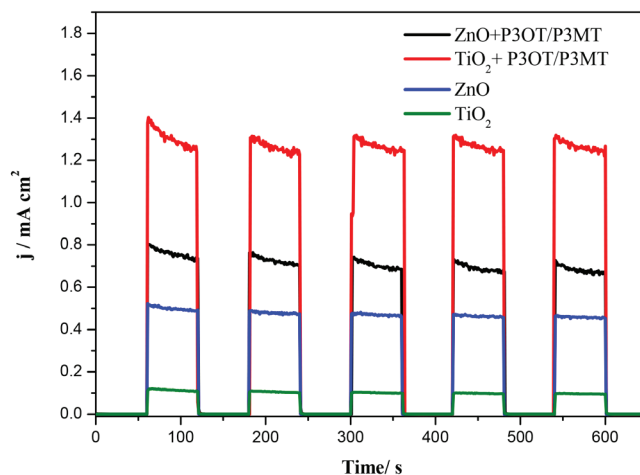


**Figure 9.** Photochronoamperometry measurements for samples under 100 mW cm<sup>-2</sup> of illumination. The lamp was interrupted at a time interval of 60 s

It can be seen in Figure 9 that the TiO<sub>2</sub>+P3OT/P3MT the cell presented a photocurrent of approximately J<sub>sc</sub> = 1.4 mA cm<sup>-2</sup>, while the ZnO+P3OT/P3MT cell showed J<sub>sc</sub> = 0.8 mA cm<sup>-2</sup>. The use of the copolymer caused the photocurrent increase by 14 times to the TiO<sub>2</sub>+P3OT/P3MT cell in relation to TiO<sub>2</sub>. To the cell ZnO+P3OT/P3MT the increase was the 2 times bigger than the ZnO, proving the high electron injection capacity of the surface of the semiconductor. These results also indicate that the interactions between TiO<sub>2</sub> and copolymers are more pronounceable when compared to ZnO film.

**Table 1.** Parameters obtained from the j-V curves of TiO<sub>2</sub> and ZnO cell sensitized with copolymer P3OT/P3MT

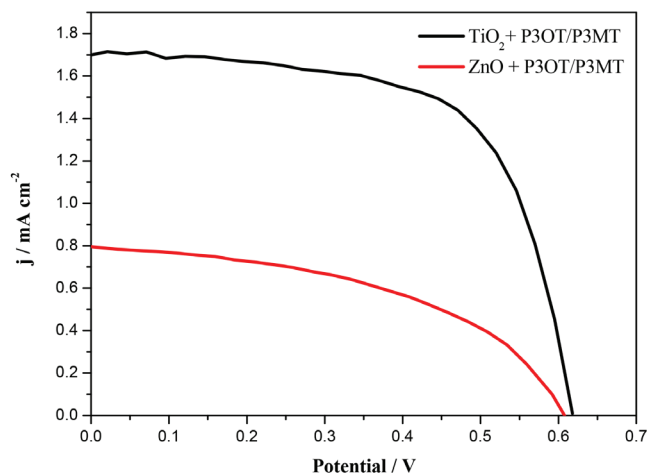
Semiconductor	J <sub>sc</sub> (mA cm <sup>-2</sup> )	V <sub>oc</sub> (V)	FF	η (%)
TiO <sub>2</sub>	1.545 ± 0.240	0.615 ± 0.004	0.637 ± 0,003	0.617 ± 0.117
ZnO	0.719 ± 0.109	0.623 ± 0.024	0.496 ± 0,033	0.215 ± 0.035

As related by Gratzel,<sup>27</sup> the size of the particle is a limiting factor in the production of charge injection in third generation of photovoltaic systems. When reaching nanometric dimensions, the materials acquire new mechanical, electrical, chemical and optical properties, because a confinement of electrons occurs in their interior, making their properties more accentuated. Among them, the increase of the surface area of the particles and a greater porosity, allows larger amounts of polymer adsorbed, generating high efficiency solar cells.

It was also verified that all systems presented a high on/off ratio and fast switching because when light impinged on the cell, the current increase was instantaneous, and when the lamp was interrupted, the current for both systems was close to zero. This proves that the reactions that govern the device are extremely fast. Regarding the stability of the devices, it was verified that both remained stable during the analysis period.

Only small current decays were observed, which are related to the diffusion processes at the interface of the device. According to Valério *et al.*<sup>28</sup> and Essner,<sup>29</sup> the rate of reduction of the triiodide ions at the cathode does not follow the oxidation rate of the iodide ions at the anode, so some polymer molecules remain in the oxidized state until a triiodide molecule can reach the oxide to reduce it. At the moment the reduced species of the electrolyte arrives at the surface of the anode is immediately oxidized without being able to penetrate the porous oxide, so the polymer molecules that are in the deeper layers of the oxide remain oxidized and the drop in current can be observed, however, after a few seconds, J<sub>sc</sub> stabilized.

Figure 10 shows j-V plots of the cells which were analyzed.

**Figure 10.** Typical j-V curves obtained from the cells analyzed under 100 mW cm<sup>-2</sup> of simulated solar irradiation

Using the results shown in Figure 10, it was possible to determine the photovoltaic parameters of the devices listed in Table 1 and calculate the energy conversion efficiency (η) using Equation 1, being that, V<sub>oc</sub> = open-circuit potential, J<sub>sc</sub> = short-circuit current, FF = fill factor and P<sub>in</sub> = solar irradiation, of 100 mWcm<sup>-2</sup>.<sup>30</sup>

$$\eta = \frac{J_{sc} V_{oc} FF}{P_{in}} \times 100\% \quad (1)$$

The current is associated with the electron injection mechanism and the charge carrier transport. It reaches its maximum when the electric voltage is zero and when a potential is applied, the current decays, as there is an increase in the resistance.<sup>14</sup> It was observed that the cells presented a high V<sub>oc</sub> of 0.615 ± 0.004 V and 0.623 ± 0.024 V for TiO<sub>2</sub> and ZnO, respectively, similar to the values found for cells using high-performance photoelectrochemical dyes. Guimaraes *et al.*<sup>22</sup> reached values of V<sub>oc</sub> = 0.600 V and V<sub>oc</sub> = 0.610 V for TiO<sub>2</sub> devices using ruthenium-based dyes.

The excellent fill factor results for the TiO<sub>2</sub> cell should also be noted. The FTO/TiO<sub>2</sub>/P3OT-P3MT system presented values of FF = 0.617 ± 0.117, approaching the best values found when using ruthenium-based dyes as photosensitizers (FF ~ 0.7).<sup>31</sup>

The cell with the highest energy conversion efficiency was produced with the anode interface FTO/TiO<sub>2</sub>/P3OT-P3MT, yielding approximately 0.617% ± 0.117. It is observed that the efficiency values obtained are closely related to the photocurrent density generated by the system since the ZnO cell presented a photocurrent (J<sub>sc</sub> = 0.719 ± 0.109 mA cm<sup>-2</sup>) about 47% lower than that of the TiO<sub>2</sub> cell (J<sub>sc</sub> = 1.545 ± 0.240 mA cm<sup>-2</sup>). The efficiency may also be associated with the morphology of the oxide used. Since TiO<sub>2</sub> presented a smaller particle size, it has a higher surface area available for the adsorption of the polymer. With increased adsorption, the flow of electrons during the operation of the solar cell is consequently increased. The copolymer was able to form electron-hole pairs, as improved photocurrent values were obtained, proving that it is efficient in charge injection.<sup>32-34</sup>

## CONCLUSION

The X-ray diffractograms showed high purity and crystallinity of both oxides, TiO<sub>2</sub> and ZnO, which exhibited anatase and wurtzite hexagonal phases, respectively. The SEM images demonstrated the spherical morphology of ZnO, while TiO<sub>2</sub> formed agglomerates because of its high surface area and small particle size.

Electrochemical characterization of the cells indicated TiO<sub>2</sub> as the best oxide for use in solar cells sensitized by copolymers, since this cell presented lower charge transfer resistance, as determined by electrochemical impedance spectroscopy (EIS), and a higher current density value j<sub>TiO<sub>2</sub></sub> = 1.545 mA cm<sup>-2</sup>, achieving an efficiency of 0.617%. The copolymer proved to be a satisfactory charge donor, as photochronoamperometry experiments showed an increase of 14 times in the current for the TiO<sub>2</sub> cell and 2 times for ZnO when compared to non-sensitized oxides.

## ACKNOWLEDGMENT

This study was financed in part by the Coordenação de Aperfeiçoamento de Pessoal de Nível Superior – Brasil (CAPES) – Finance Code 001. Acknowledgment to CNPq, SETI/UGF, FINEP.

## REFERENCES

- Freitas, J. N.; Pivrikas, A.; Nowacki, B.; Akcelrud, L. C.; Sariciftci, N. S.; Nogueira, A. F.; *Synth. Met.* **2010**, *160*, 1654.

2. Alwani, M. A. M.; Mohamad, A. B.; Ludin, N. A.; Kadum, A. A. H.; Sopian, K.; *Renewable Sustainable Energy Rev.* **2016**, *65*, 183.
3. Yun, S.; Freitas, J. N.; Nogueira, A. F.; Wang, Y.; Ahmade, S.; Wang, Z-S.; *Prog. Polym. Sci.* **2015**, *59*, 1.
4. Vitoreti, A. B. F.; Vaz, R.; Pena, A. L.; Raphael, E.; Ferrari, J. L.; Schiavon, M. A.; *Rev. Virtual Quim.* **2017**, *9*, 4.
5. Shoaee, S.; Briscoe, J.; Durrant, J. R.; Dunn, S.; *Adv. Mater.* **2014**, *26*, 263.
6. De Santana, H.; Maia, E. C. R.; Bento, D. C.; Cervantes, T. N. M.; Moore, G. J.; *J. Mater. Sci.: Mater. Electron.* **2013**, *24*, 3352.
7. Maia, G. A. R.; Larsson, L. F. G.; Viomar, A.; Matos, L. A. C.; Antunes, S. R. M.; Maia, E. C. R.; Oliveira, M. F.; Cunha, M. T.; Rodrigues, P. R. P.; *J. Mater. Sci.: Mater. Electron.* **2016**, *27*, 8271.
8. de Freitas, J. N.; Li, R. W. C.; Nogueira, A. F.; Gruber, J.; *Mater. Chem. Phys.* **2011**, *130*, 223.
9. Kashyout, A. B.; Soliman, M.; el Gamal, M.; Fathy, M.; *Mater. Chem. Phys.* **2005**, *90*, 230.
10. Parussulo, A. L. A.; *Tese de Doutorado*, Universidade de São Paulo, Brasil, 2013.
11. Pereira, É. A.; Montanhera, M. A.; Spada, E. R.; Paula, F. R.; *21º CBECIMAT - Congresso Brasileiro de Engenharia e Ciência dos Materiais*, Cuiabá, Brasil, 2014.
12. Oliveira, P. L.; Araújo, D. S.; Costa, A. C. F. M.; Oliveira, L. S. C.; *22º CBECiMat - Congresso Brasileiro de Engenharia e Ciência dos Materiais*, Natal, Brasil, 2016.
13. Gusatti, M.; Rosário, J. A.; Barroso, G. S.; Campos, C. E. M.; Riella, H. G.; Kunhen, N. C.; *Chem. Eng. Trans.* **2009**, *17*, 1017.
14. Maia, G. A. R.; Larsson, L. F. G.; Viomar, A.; Maia, E. C. R.; de Santana, H.; Rodrigues, P. R. P.; *Cerâmica (Sao Paulo, Braz.)* **2016**, *62*, 361.
15. Hermínio, D. F.; *Dissertação de Mestrado*, Universidade Federal de Pernambuco, Brasil, 2012.
16. Li, D.; Haneda, H.; *Chemosphere* **2003**, *51*, 129.
17. Fan M.; Jing Y.; Yue-Qin D.; Zhi-Hao Y.; Li-Jian B.; *Sens. Actuators, B* **2011**, *156*, 703.
18. Mayrinck, C.; Rocha, L. A.; Vitoreti, A. B. F.; Vaz, R.; Tartuci, L. G.; Ferrari, J. L.; Schiavon, L. A.; *Rev. Virtual Quim.* **2017**, *9*, 717.
19. Costa, A. C. F. M.; Ramalho, M. A. F.; Neiva, L. S.; Alves-Jr. S.; Kiminami, R. H. G. A.; Gama, L.; *Revista Eletrônica de Materiais e Processos* **2007**, *2.3*, 14.
20. Pratsinis, S. E.; *Prog. Energy Combust. Sci.* **1997**, *24*, 197.
21. Hong, R. Y.; Li, J. H.; Chen, L. L.; Liu, D. Q.; Li, H. Z.; Zheng, Y.; Ding, J.; *Powder Technol.* **2009**, *189*, 426.
22. Muniz, E. C.; Goes, M. S.; Silva, J. J.; Varela, J. A.; Joanni, E.; Parra, R.; Bueno, P. R.; *Ceram. Int.* **2011**, *37*, 1017.
23. Guimaraes, R. R.; Paurussulo, A. L. A.; Matias, T. A.; Toma, H. E.; Araki, K.; *Electrochim. Acta.* **2017**, *255*, 92.
24. Ricchariya, G.; Kumar, A.; *Opt. Mater.* **2018**, *79*, 296.
25. Ghan, W.; Kang, H.; Sheikh, T.; Yadav, S.; Gil, T. C.; Nesbitt, F.; Uddin, J.; *Sci. Rep.* **2017**, *7*, 41470.
26. Latif, M. S. A.; Abuiridan, M. B.; Dahoudi, N. A.; Kahlout, A. M.; Taya, S. A.; Agez, T. M.; Ghamri, H. S.; *Science, Technology and Development* **2015**, *34*, 135.
27. Grätzel, M.; *Nature* **2001**, *414*, 338.
28. Valério, T. L.; Maia, G. A. R.; Viomar, A.; Dias, B. V.; Rodrigues, P. R. P.; *Orbital: Electron. J. Chem.* **2018**, *10*, 234.
29. Essner, J.; *Dissertação de Mestrado*, Kansas State University, Estados Unidos, 2011.
30. Narayan, M. R.; *Renewable Sustainable Energy Rev.* **2012**, *16*, 208.
31. Zhao, J.; Wu, J.; Zheng, M.; Huo, J.; Tu, Y.; *Electrochim. Acta.* **2015**, *156*, 261.
32. Wongcharee, K.; Meeyoo, V.; Chavadej, S.; *Sol. Energy Mater. Sol. Cells.* **2007**, *91*, 556.
33. Kumara, N. T. R. N.; Ekanayake, P.; Lim, A.; Iskandar, M.; Ming, L. C.; *J. Sol. Energy Eng.* **2013**, *135*, 031014.
34. Sonai, G. G.; Melo, M. A.; Nunes, J. H. B.; Megiatto Jr., J. D.; Nogueira, A. F.; *Quim. Nova* **2015**, *38*, 1357.